Local Probe Oxidation of Self-Assembled Monolayers on Hydrogen-Terminated Silicon

Menglong Yang,[†,‡,¶] Daan Wouters,[§,⊥,¶] Marcel Giesbers,[†] Ulrich S. Schubert,[§,∥,*] and Han Zuilhof[†,*]

[†]Laboratory of Organic Chemistry, Wageningen University, Dreijenplein 8, 6703 HB Wageningen, The Netherlands, [‡]Qingdao Institute of Bioenergy and Bioprocess Technology, Chinese Academy of Sciences, 266101 Qingdao, People's Republic of China, [§]Laboratory of Macromolecular Chemistry and Nanoscience, Eindhoven University of Technology, 5600 MB Eindhoven, The Netherlands, [⊥]Dutch Polymer Institute (DPI), P.O. Box 513, 5600 MB Eindhoven, The Netherlands, and [∥]Laboratory of Organic and Macromolecular Chemistry, Friedrich-Schiller-University Jena, Humboldtstrasse 10, D-07743 Jena, Germany. [¶]These authors contributed equally to this work.

ABSTRACT Local probe oxidation experiments by conductive AFM have been performed on a hexadecyl monolayer and a *N*-hydroxysuccinimide (NHS)-ester-functionalized undecyl (NHS-UA) monolayer assembled on hydrogen-terminated (*i.e.*, unoxidized) silicon. The oxidation conditions for the mild oxidation of the top terminal groups of monolayers and the deep oxidation of the underlying silicon into silicon oxide were investigated. The results show that the bias threshold for the AFM tip-induced oxidation of the top groups of monolayers on oxide-free silicon can be reduced by 2 V for the methyl-terminated hexadecyl monolayer and even by 3.5 V for the active NHS-ester-terminated undecyl monolayer, in comparison to a methyl-terminated octadecyl trichlorosilane (OTS) monolayer on oxidized silicon. Upon such local mild oxidation, the active NHS ester group of the NHS-UA monolayer is selectively cleaved off to generate carboxyl-containing monolayer nanopatterns, opening further possibilities for subsequent patterned multifunctionalization.

KEYWORDS: local probe oxidation · nanolithography · nanopatterning · self-assembled monolayer (SAM) · hydrogen-terminated silicon · *N*-hydroxysuccinimide (NHS) · XPS analysis

The local oxidation of silicon to silicon oxide[1,2] has been presented as an alternative method to conventional silicon patterning technology since the formed silicon oxide patterns can be used in subsequent wet-etching steps.[3] For application in sensor devices, nanoscale patterns with chemically active surfaces as well as methods that allow site-selective positioning or modification of these active sites are required. Local probe oxidation can, in principle, be used for site-selective surface modifications[4] to obtain surface functionalities that can otherwise only be obtained upon the patterned deposition of functionalized self-assembled monolayers (SAMs).[5,6] Such organic monolayers are usually used as resist materials in local probe oxidation experiments.[7,8] Sagiv and coworkers introduced the concept of electro-oxidative patterning of the monolayer itself.[9] By applying a suitable bias voltage, the vinyl end groups of a self-assembled silane monolayer can be oxidized into carbonyl-containing end groups, typically with both carboxylic acid (−COOH) and aldehyde (−CHO) moieties. This creates the possibility to prepare chemically active surface patterns that can be used in subsequent surface modification steps.[10,11] The local probe oxidation of octadecyl trichlorosilane (OTS) monolayers initiates voltage-dependent reactions: (1) at high bias voltages, the monolayer undergoes oxidative degradation, which is accompanied and followed by the formation of silicon oxide (SiO_x), or (2) at intermediate voltages, carboxylic-acid-containing surface patterns[12] are generated, which can be used in a large number of subsequent surface modification reactions.[10,13]

Despite the fact that the local probe oxidation of self-assembled monolayers of OTS has been demonstrated to be a powerful and versatile method, its application in sensor devices is limited because of the use of silanes (*e.g.*, trichlorosilanes, trimethoxy or triethoxy silanes) as precursors for the formation of monolayers. Since self-assembled monolayers of silanes are anchored on the hydroxylated silica surface *via* cross-linked Si−O−Si bonds, the relatively low chemical stability of the attachment layer does not tolerate basic reaction media. This limits subsequent surface modification reactions. In addition, the silica layer possesses a high density of electrically active defects, which degrade the electrical characteristics of the underlying semiconductor silicon. Furthermore, the high water sensitivity of silanes demands a very strict process control in the monolayer formation to ensure a uniform monolayer, while the highly reactive silanes themselves are also incompatible with a large number of functional groups (*e.g.*, hydroxyl and carboxyl).

*Address correspondence to ulrich.schubert@uni-jena.de, han.zuilhof@wur.nl.

Received for review November 11, 2008 and accepted September 1, 2009.

Published online September 16, 2009.
10.1021/nn9007059 CCC: $40.75

Several alternatives to SAMs of silanes on hydroxylated silica surfaces exist, specifically organic monolayers covalently attached onto a oxide-free hydrogen-terminated silicon (H-silicon),[14−16] among which Si−C linked alkyl monolayers have been extensively studied.[17] Such alkyl monolayers can be formed by the hydrosilylation of H-silicon by primary alkenes or alkynes, which yields a densely packed monolayer directly bonded onto silicon *via* the formation of Si−C bonds.[18−20] Ongoing developments in the past decade have made the formation conditions of alkyl monolayers on silicon milder and milder and compatible with the presence of a wide variety of functional groups (including carboxylic acids[21,22]) at the tail end of the 1-alkene or alkyne molecules.[17,19] High-quality organic monolayers can be routinely prepared by thermal reactions,[23,24] UV activation,[25] visible-light irradiation,[26−28] and—as has been shown recently—even at room temperature in the dark.[29] The highly stable Si−C linkage layer can tolerate mildly basic reaction media,[30] while the absence of any silica layer yields a low density of electrically active defects in the interface between the monolayer and semiconductor substrate.[31−41]

Like local oxidation experiments for OTS monolayers on oxidized silicon, local probe oxidation experiments have also been reported for Si−C bonded alkyl monolayers on unoxidized silicon enabling the fabrication of functional nanopatterns.[42−44] In these reports, the alkyl monolayers were used as resists and were completely degraded in locally oxidized domains to open the window for subsequent etching procedures. The influence of oxidation parameters such as bias voltage and oxidation duration on the formation of silicon dioxide was studied.[45−47] Furthermore, preliminary results on the AFM tip-induced mild oxidation of the monolayer itself were reported for an oligo(ethylene glycol) (OEG)-terminated monolayer on unoxidized silicon.[48]

Here, we report in detail on the local oxidation of the covalently Si−C linked monolayers themselves. By systematic variation of the bias voltage and the length of the oxidation duration, the threshold for the monolayer surface oxidation was studied, as well as the monolayer degradation and the simultaneous formation of silicon oxide. In addition, for the first time, local probe oxidation experiments were performed on chemically reactive monolayers bearing *N*-hydroxysuccinimide (NHS)-activated carboxylic acid groups at the top of the organic monolayers. Upon application of a suitable bias voltage, the highly amine-reactive NHS ester end group is expected to be cleaved off, generating nanopatterns with less amine-reactive carboxylic-acid-terminated surfaces as a "negative-tone" template for the subsequent assembly of amines. Such a template is characterized as negative-tone because, in subsequent modifications, the surrounding matrix surface will be selectively functionalized *via* coupling with amines, leaving nanodomains available for further modification. This complements the approach of Fresco *et al.* who use probe oxidation on unreactive precursor monolayers to deprotect protected amine and thiol end groups, and thus form "positive-tone" templates terminated with reactive amine and thiol end groups.[49,50]

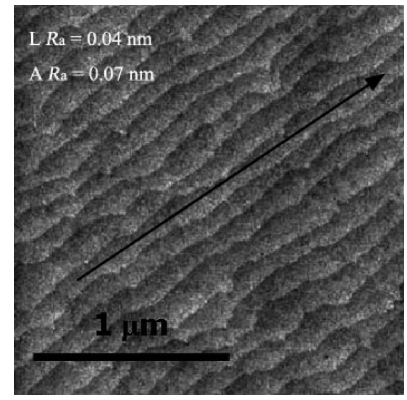

Figure 1. Tapping-mode height images of a hexadecylated silicon (111) surface displaying wide atomically flat terraces. Average line roughness (L R_a) (along the arrow) and average area roughness (A R_a) over the whole measured surface are indicated in the image.

RESULTS AND DISCUSSION

Densely packed hexadecyl and NHS ester undecyl (NHS-UA) monolayers were prepared on a flat hydrogen-terminated Si(111) surface by hydrosilylation with 1-hexadecene[26−28] or *N*-succinimidyl undecylenate.[51] Figure 1 displays an AFM tapping-mode height image of a hexadecylated silicon surface (the height image of NHS-UA monolayers is similar, shown in Figure S1 in the Supporting Information). The micrograph in Figure 1 shows approximately 100 nm wide atomically flat terraces with an average line roughness of 0.04 nm on the terrace surfaces and an average area roughness of 0.07 nm over the whole measured surface, reflecting an ideal interface topography of the underlying Si(111) substrate. The chemical composition of these monolayers was confirmed by X-ray photoelectron spectroscopy (XPS) (*vide infra*; Figure S2 in the Supporting Information and Figure 9a). Much like self-assembled monolayers of octadecyl trichlorosilane (OTS) on SiO_2/Si, hexadecyl monolayers are hydrophobic (static water contact angle ∼109°) and chemically inert. In contrast, NHS-UA monolayers are fairly hydrophilic (static water contact angle ∼65°) and very reactive toward amines.[51,52]

To test whether the process of local electro-oxidation of monolayers is also possible on alkylated silicon substrates, an electrically biased Pt-coated AFM probe (tip radius ∼ 35 nm and a standard contact-mode cantilever with spring constant k ∼ 0.03 N/m) was used in contact mode to oxidize patterns on hexa-

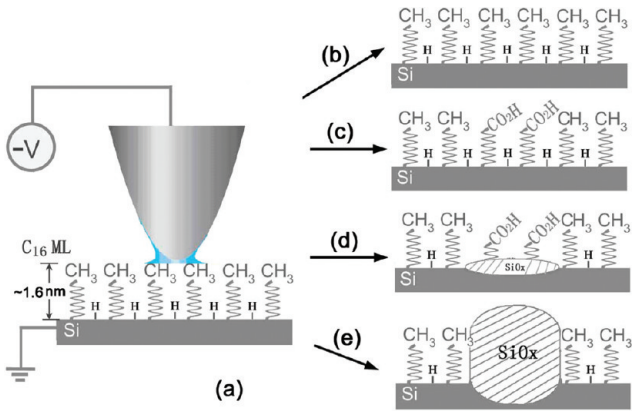

Figure 2. Effects of applied voltage biases and duration of the oxidation pulse. Depending on the bias voltage and oxidation duration, the local oxidation of an alkyl monolayer on silicon (a) may result in no oxidation (b), oxidation of the monolayer (c), monolayer degradation combined with silicon oxidation (d), and continuous growth of bare silicon oxide after complete degradation of monolayer (e). The thickness of a hexadecyl monolayer was reported as ~1.6 nm.[53]

decylated silicon surfaces. Contact-mode AFM imaging in both height and friction mode was used to observe possible changes within the monolayer after patterning with varying bias voltage and duration of the oxidation. It was expected that upon the local electro-oxidation of the alkylated silicon substrates four sequential effects may be observed depending on the bias voltage and duration of the oxidation pulse. As schematically illustrated in Figure 2, for low voltages, these monolayers remain unchanged (Figure 2b), whereas for a narrow range of increased bias voltages and oxidation durations, mild oxidation of monolayers appears. In this range, carboxylic acid (−COOH) end groups are formed upon the oxidation of the methyl end groups of monolayers (possibly combined with the oxidative degradation of several top methylene groups in monolayers, while the underlying silicon remains unoxidized (Figure 2c). Subsequently, there may exist a narrow range of bias voltages and oxidation durations in which oxidation can result in serious but incomplete monolayer degradation, simultaneously accompanied by the oxidation of the underlying silicon (Figure 2d). At even higher voltages and longer oxidation durations, the monolayer is completely degraded, followed by the growth of bare silicon oxide (Figure 2e).

Figure 3 displays local probe oxidation experiments on a hexadecyl monolayer-coated silicon substrate. The contact-mode height and friction images were recorded in both trace (left column) and re-trace (right column) directions. A set of circles or crosses was patterned by varying biases and pixel durations (detailed in Experimental Section). Since the pixel duration (*i.e.*, the length of oxidation duration per pixel) is inversely proportional to the speed with which the tip moves, using a fixed pixel resolution, the pixel duration can be scaled to the overall oxidation time per unit length, as indicated in the top-left one of each grouped images. Many small dot-like features observed in the friction images on the background surface can be attributed to the absorption of oxygen-rich airborne contaminations onto the monolayer surface, in line with the excess oxygen content in the monolayer as measured by XPS (Figure S2 in the Supporting Information).

The different oxidation results can be identified by the differences in height and friction images between trace and re-trace directions. For example, for this paper, the most interesting situation of monolayer oxidation (Figure 2c) was realized by applying −6 V (the voltage of the biased AFM tip relative to the sample substrate) biases on the hexadecyl monolayer. After the local probe oxidation, both the −6 V circle (2.5 ms pixel duration; Figure 3a) and the −6 V cross (2.0 ms pixel duration; Figure 3b) show up with a clear friction contrast in both trace and re-trace scan directions. As expected, these sig-

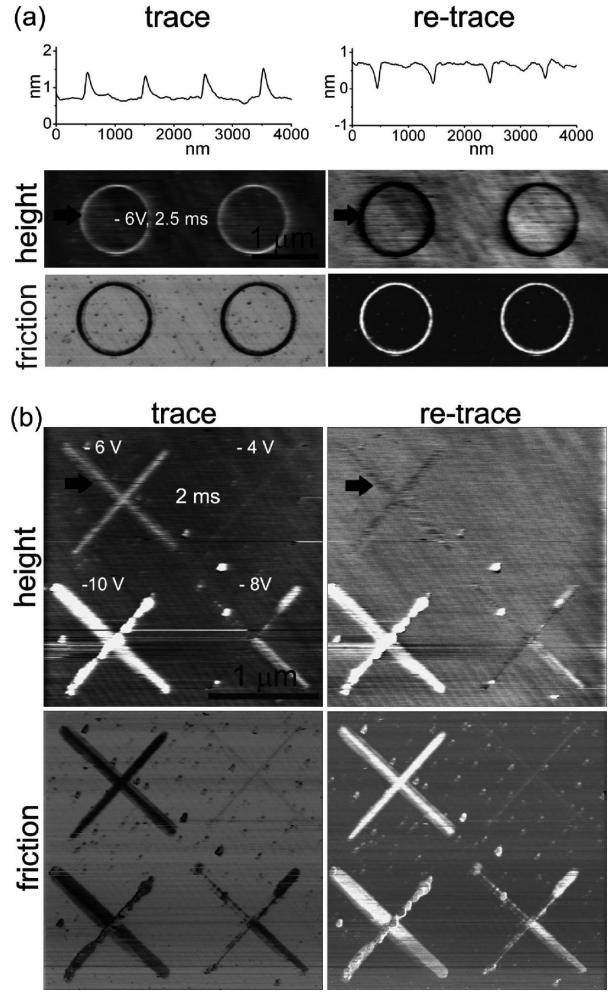

Figure 3. Contact-mode AFM height and friction images of a patterned hexadecylated silicon surface. (a) Two circles showing monolayer oxidation (−6 V bias at a pixel duration of 2.5 ms), and section profiles along the arrow above the height images. (b) Set of crosses obtained by different biases (indicated in the top-left height image) at a pixel duration of 2.0 ms. (All patterns were obtained in a pixel resolution of ~205 pixels/μm.)

nals change contrast upon reversal of the scan direction from trace to re-trace. However, in the height images, they display a positive height contrast in the forward scan direction, but a negative height contrast in the reverse direction (Figure 3a, top; see arrows for position of scanned features). The baseline widths of the oxidized features are about 80 nm, in line with the tip radius of ~35 nm. This reversed height contrast has been observed previously for oxidized OTS monolayers[12] and originates from an artifact in the contact-mode AFM imaging caused by the cross-correlation between height and friction signals. For OTS monolayers, this is only observed for the oxidation of the monolayers (resulting in the formation of oxygen-rich end groups, typically −COOH), and this feature will be used here to identify the oxidation of hexadecyl monolayers on unoxidized silicon, as well. A more detailed description of AFM imaging artifacts and their application to the characterization of monolayer oxidation has been reported elsewhere.[12,45]

More oxidation results are displayed in Figure 3b. The cross inscribed at −10 V bias (2 ms pixel duration) shows up with a clear positive height contrast in both trace and re-trace scan directions and with clear friction contrasts in both scan directions. In contrast to the positive/negative reserved height contrasts for −6 V patterns, the unchanged positive height contrast confirms the formation of silicon oxide in the −10 V oxidized domains. A −8 V bias produced an oxidation appearance between the effects of −10 and −6 V; a part of the cross inscribed at −8 V is observed with significantly positive heights, while the rest shows small negative heights in both trace and re-trace height images. This can be explained by local defects or a decreased packing density of the monolayer chains with a big loss in height caused by significant degradation of the monolayer. This result indicates that the −8 V bias is strong enough to cause the degradation of the monolayer and the formation of silicon oxide. However, its efficiency to oxidatively form silicon oxide is clearly lower than the −10 V bias and is also possibly more easily affected by changes in the tip conductivity during the oxidation experiment. Finally, a bias of −4 V is too weak to cause reliable changes in both height and friction images and thus cannot be used for the local oxidation of the monolayer, although a −4 V bias can sometimes induce—without reliable reproducibility—a weak frictional signal, as shown in Figure 3b.

To detail the dependence of the oxidation result for hexadecyl monolayers on the bias voltage and pixel duration, the experiment displayed in Figure 3 was repeated with varying bias voltages and pixel durations. After local probe oxidation, the patterned areas were imaged by contact-mode AFM in both trace and re-trace scan directions. The oxidation conditions and results are summarized in Figure 4. Similar results were obtained on octadecyl monolayers, and on these substrates, the nature of the oxidized features was confirmed by HF-etching experiments (see Supporting Information, Figures S5 and S6). It was observed that the results of the oxidation pulse depend strongly on the tip quality. For example, the exact position of oxidation thresholds varied only slightly between new tips (typically <0.5 V) but rather substantially (up to 1.5 V) between worn ones. Some border conditions indicated by cross (×) in Figure 4 display these variable results. Our previous results also demonstrated that an AFM tip undergoing different wearing degrees could induce silicon oxide lines in remarkably different heights and widths even under the same probe oxidation conditions.[46] The dependence of oxidation results on worn tips is mainly ascribed to the fact that the wearing can change the tip geometry and degrade the tip conductivity,[54] thus reshaping the water meniscus and the electric field between the biased tip and the substrate.[55]

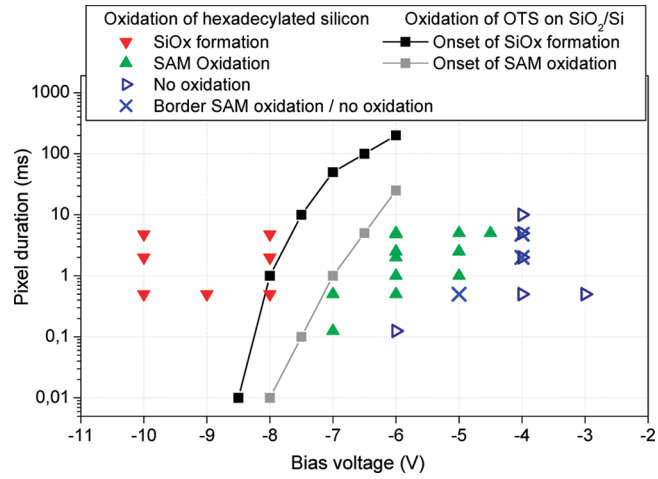

Figure 4. Oxidation results for the local probe oxidation on a hexadecyl monolayer on Si (scatter plots) as a function of applied bias and pixel duration (oxidation was performed with a resolution of ~205 pixel/μm). The oxidation results on an octadecyl trichlorosilane (OTS) monolayer on SiO_2/Si (dot-and-line)[12] are included for comparison.

For a rough comparison, two series of black and gray dots and lines were added in Figure 4 to indicate the oxidation results for an OTS monolayer on SiO_2/Si, as described earlier.[12] The black line and gray line show the threshold conditions for the formation of silicon oxide patterns and carboxyl-terminated monolayer patterns on OTS/SiO_2/Si, respectively. At conditions left of the black line, thick silicon oxide features are formed that stick out about the surrounding OTS monolayer, whereas at conditions right of the gray line, no oxidation is observed. Between the black line and gray line, a narrow oxidation window exists, in which the top end groups of OTS monolayers are oxidized into carbonyl-containing end groups. In order to unambiguously distinguish monolayer oxidation from the conditions that also yield silicon oxidation, the oxidation on hexadecy-

lated silicon was mainly studied under oxidation conditions on the right of the gray line and on the left of the black line.

Depending on the height effects observed by contact-mode AFM, the oxidation results on hexadecylated silicon can be classified as follows: (1) no oxidation (see Figure 2b; indicated by blue rightward-triangles), in case no change in the monolayer was observed; (2) formation of silicon oxide (Figure 2e; red down-triangles), in case a positive height was found in both scan directions; and (3) monolayer oxidation (Figure 2c; green up-triangles), *i.e.*, formation of carboxylic acid end groups due to the oxidation of top methyl groups possibly involving the oxidative degradation of several top methylene groups, in case a change in sign (positive/negative) in observed height was found upon changing scan direction.

Theoretically, the situation for Figure 2d can display different kinds of apparent features. In one extreme, the increase in height from the formation of silicon oxide significantly dominates over the height loss from the monolayer degradation, and contact-mode AFM will thus measure features like those depicted in Figure 2e (*i.e.*, positive heights in both trace and re-trace scan directions), which are classified as silicon oxide formation. In the opposite extreme, AFM-measured apparent heights may appear like those for the situation in Figure 2c, and the oxidation results may be classified as oxidative monolayer degradation. In principle, contact-mode AFM cannot sharply distinguish situation 2d from situation 2c or 2e.

In view of the results obtained for the local oxidation for OTS monolayers on SiO_2/Si, Figure 4 indicates that all bias conditions on the left of the black line can cause silicon oxidation from the hexadecylated silicon, whereas the bias range on the right of the gray line can cause monolayer oxidation where no oxidation from OTS/SiO_2/Si can be observed. Compared to the OTS monolayer-coated SiO_2/Si, the bias threshold to initiate the oxidation of methyl end groups (into carboxyl-containing end groups) on the surface of hexadecyl monolayers on silicon is obviously lowered, by about 2 V, decreasing to −4.5 V (as indicated by green up-triangles in Figure 4). This decrease of the bias threshold for monolayer oxidation makes local oxidation of alkyl monolayers on unoxidized silicon more selective toward functional groups in the monolayer than for the corresponding silane-based monolayers on oxidized silicon. The lowering of the monolayer oxidation threshold for hexadecylated silicon compared to OTS/SiO_2/Si can be ascribed to the enhancement of the effective electric-field intensity between the biased tip and the monolayer surface due to the absence of the insulating silicon dioxide layer as well as the reduced monolayer thickness.[6] The effect of the silicon dioxide layer was detailed by an additional experiment: even a −10 V bias could not realize the oxidation of an OTS monolayer on a thermally oxidized silicon substrate (a Si wafer was oxidized at 900 °C for 48 h to form a thick oxide layer before the self-assembly of OTS). In addition, the detailed probe oxidation results will likely also depend on the doping type and concentration of Si substrates,[56−58] which have not yet been studied on monolayer-modified Si.

Besides the lower bias threshold for monolayer oxidation and the higher chemical stability of the covalently bound Si−C linkages between the alkyl chains and the silicon substrate, the biggest advantage of Si−C linked monolayers on unoxidized silicon, in comparison to silane SAMs on oxidized silicon, is that the attachment conditions for Si−C linked monolayers are compatible with a much wider diversity of functional groups at the top surface. Since silanes, and especially chlorosilanes, are highly reactive and polymerize upon exposure to water (moisture) and hydroxyl groups, the number of commercially available chlorosilanes with functional groups at the terminal end of the silane molecule is rather limited. For example, carboxylic acid and its *N*-hydroxysuccinimide (NHS) ester are two very useful terminal groups to biofunctionalize the monolayer surface, but thus far, no silanes with either of these two terminal groups are commercially available. In contrast, carboxylic-acid-terminated[21,22] and/or corresponding NHS-ester-terminated 1-alkenes[51,52] or 1-alkynes[29] can be routinely bonded directly onto H-silicon in a light-induced attachment,[25−28] resulting in Si−C linked monolayers terminated with the carboxyl acid and/or corresponding NHS ester end groups.

To pattern monolayers bearing chemically functional groups at the top surface, NHS-UA (the NHS ester of 10-undecenoic acid) monolayers were used for local probe oxidation (schematically shown in Figure 5). The NHS-activated acid groups are highly reactive and will readily react at room temperature with, for example, amines. Upon exposure to a local bias voltage, the succinimide group is expected to be cleaved off, resulting in the formation of less reactive carboxylic acid end groups as a negative-tone template to amine-terminated molecules.

As demonstrated for hexadecylated silicon, overoxidation to yield silicon oxide was expected to be also possible for NHS-ester-terminated monolayers on silicon. To optimize the oxidation conditions, a series of concentric dicircle patterns onto the NHS-UA monolayer on silicon were obtained using local probe oxidation with varying voltages (see Figure 6). However, due to the high polarity of the NHS ester moieties resulting in the presence of large snap-in and snap-out forces toward the AFM tip, the usual contact-mode soft cantilever (like previously used for hexadecyl monolayer surfaces) could not be used to reproducibly oxidize and/or image NHS-ester-terminated surfaces. Therefore a Pt-coated AFM probe with a stiffer cantilever (with $k \sim$ 0.95 N/m and $f \sim$ 105 kHz, suitable for tapping mode

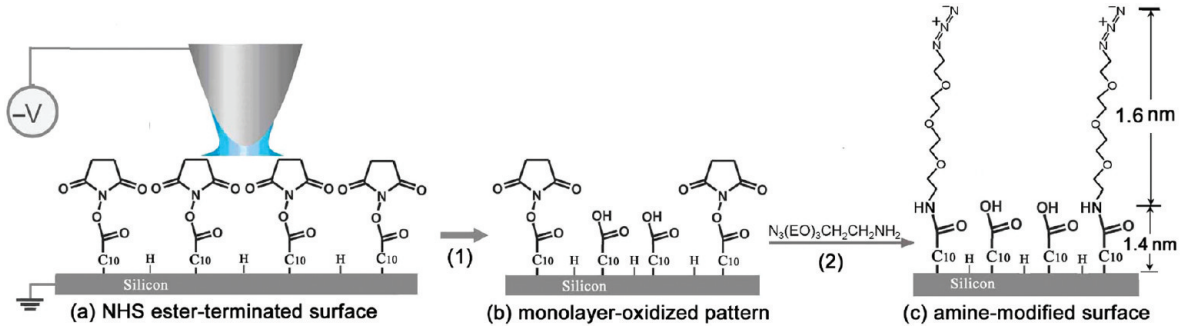

Figure 5. Schematic representation of the mild local oxidation of an NHS-UA monolayer and the subsequent functionalization reaction with $N_3-(EO)_3-NH_2$, resulting in a local height increase.

as well as contact mode; tip radius ~25 nm) was used in different modes for probe oxidation and imaging experiments on NHS-ester-terminated surfaces. Only the oxidation was performed in contact mode (without preimaging of the substrate to minimize possible damaging by the large interaction forces between the NHS-ester-terminated surface and the AFM tip), while the subsequent imaging was done in tapping mode.

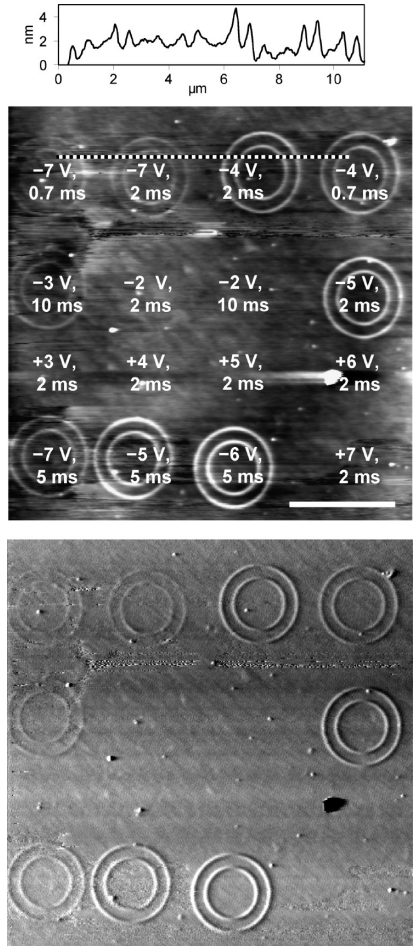

Figure 6. Tapping-mode AFM height (middle) and phase (bottom) images of oxidation results on a NHS-UA monolayer on silicon, and cross-section (top) across the dotted line in the height image. Oxidation was carried out at a pixel resolution of 171 pixels/μm. Oxidation bias voltage and pixel duration are indicated in the height image; scale bar = 4 μm.

Figure 6 displays tapping-mode height and phase images of a patterned NHS-UA monolayer onto which 16 sets of circles were inscribed using different voltages and pixel durations as indicated in the figure. From the micrographs in Figure 6, it can be concluded that at positive voltages on the tip (*i.e.*, the substrate is relatively at negative bias) no changes occur for the NHS-UA monolayer, which agrees with a reaction mechanism by electrochemical oxidation[59,60] rather than by the thermal effects of the electric current. This observation also rules out the possibility that the mechanical interaction between the biased tip and substrate causes topographic changes of the monolayer surfaces under our experimental conditions. At negative voltages, a −3 V bias for 10 ms results in just observable changes (apparent height changes ≤0.3 nm in height image and weak contrasts in the phase image) for this NHS-UA monolayer, while a −2 V bias for 2−10 ms induces no change. Therefore, the bias threshold for the oxidation of the NHS-UA monolayer on silicon is only −3 V, which is considerably milder than those observed for the hexadecyl monolayer on silicon (*i.e.*, more negative than −4 V). This can be ascribed to the higher chemical activity of the NHS ester end groups in comparison to methyl end groups and the more hydrophilic surface that favors the formation of the water meniscus and thus local oxidation.

More negative biases from −4 to −6 V for 0.7−5 ms result in positive apparent heights (mostly >2 nm) that increase with bias voltages and durations. However, a decrease in apparent height (average ~1 nm) appears at −7 V bias. Since in comparison to the contact-mode AFM, the tapping-mode AFM is less affected by the cross-correlation between height and friction signals, this variation in apparent heights can be hypothesized to reflect the changes in physical heights that result from the competition between the degradation of the monolayer and the oxidation of the silicon substrate.

It has to be noted that the local probe oxidation on monolayer-modified silicon is indeed a complex multistep electrochemical process. In line with several kinetic investigations on the tip-induced oxidation of monolayer-modified silicon surfaces,[45,61] the following

process is proposed: (1) the reactive species produced from the water electrolysis by the electric field between the biased tip and the substrate attack the top of the monolayer, resulting in the oxidation of top end groups, followed by (2) a gradual degradation/shortening of the monolayer until the electric field can drive the reactive species to penetrate the remaining monolayer and thus to oxidize the underlying silicon. Both steps 1 and 2 just result in monolayer oxidation, yielding a carboxyl-rich monolayer surface as depicted in Figure 2c. Subsequently, simultaneous oxidative degradation of the remaining monolayer and growth of silicon oxide yield a schematic monolayer structure as Figure 2d (step 3). This can continue until the monolayer is completely degraded as much as feasible, after which (step 4, Figure 2e) the underlying silicon continues to be oxidized until the thickness of silicon oxide finally reaches its self-limiting value. However, the relative occurrence of these situations within oxidation domains is expected to be somewhat non-uniform due to the effects of the non-uniformity of the tip−substrate electric field, structural defects in the monolayer, as well as fluctuations in the oxidation conditions. During steps 1 and 2, AFM can usually distinguish some changes in, for example, the increased friction contrast in contact mode or phase contrast in tapping mode between the oxidized domains and the surrounding hydrophobic surface. However, it is with AFM difficult to figure out the actual changes in height (even though several groups reported that AFM imaged the negative heights within the monolayer-degradation domains in some thick and dense organic monolayers[62,63]). This is due to the coupling of the tip−surface friction or adhesion force signals to the measured height signal. In step 3, the degradation of the monolayer decreases the height, while the growth of the silicon oxide increases the height. As a result, the variation of the apparent height is determined by the total effects of these two competitive oxidation processes.[45] Finally, in step 4, AFM can show the positive height of bare silicon oxide increasing linearly with oxidation voltage and logarithmically with oxidation duration.[45]

Since the NHS-terminated monolayer is thinner, less compact, and more hydrophilic than the hexadecyl monolayer on unoxidized silicon (and OTS monolayer on oxidized silicon), it can be expected that in the local probe oxidization the reactive oxyanions[59] can more easily penetrate through this monolayer. As a result, the oxidation of the underlying silicon is more easily initiated (*i.e.*, quickly yielding step 3) for NHS-modified silicon. For less densely packed or thin monolayers, the threshold value for monolayer oxidation may in fact be high enough to also cause simultaneous oxidation of the silicon, so that oxidation of the monolayer cannot occur separately from oxidation of the surface.

The above-mentioned changes in the apparent heights upon the selected different oxidation biases for NHS-terminated monolayers (Figure 6) can be explained as follows: the positive heights increasing with biases from −3 to −6 V imply the situation in step 3 (depicted in Figure 2d) in which the growth of the underlying silicon oxide is faster than the monolayer degradation. In this situation, the surface is still covered with partially degraded monolayers bearing carboxyl end groups on top of oxidized surfaces. This conclusion is supported by the decrease in apparent height at a higher bias of −7 V. This can only indicate that this −7 V bias has greatly decomposed the remaining monolayer or at least accelerated the monolayer oxidation faster than the silicon oxide growth, thus resulting in a decrease in the apparent height.

Since the above experiments show that NHS-UA monolayer does not fully prevent the underlying silicon from the oxidation under our probe oxidation conditions, the optimal approach to our aim is thus to select biases which can oxidize a NHS-UA monolayer to give a COOH-terminated surface but, at the same time, keep the decomposition of the carbon chain and the oxidation of silicon to a minimum. A feasible bias for the fabrication of carboxyl-terminated template can thus be selected from the range −3 to −6 V in combination with relative fast writing rates (*e.g.*, relative short pixel durations), as under those conditions an only partially degraded monolayer terminated with carboxyl end groups is formed.

In the case of a thin silicon oxide bump coated by a degraded monolayer that is quite soft, loose, and hydrophilic, increased interaction forces under a moving tip may be observed. As a result, AFM is not optimally suited to display the real height of the silicon oxide bump and the thickness of the degraded monolayer because of the cross-coupling effects of the friction (mainly for contact-mode AFM) or adhesion force (mainly for tapping-mode AFM) on the height signal as well as the deformation of the soft monolayer under the tip load (for both contact and tapping-mode AFM). However, the formation of a bare silicon oxide protrusion can usually be clarified by contact-mode AFM with a steady positive height that is only slightly dependent on scan settings (*e.g.*, scan direction and force-relating parameters), especially when its hydrophilic surface is surrounded by a similarly hydrophilic matrix.

In order to find out the bias threshold for the formation of bare SiO_x protrusions, oxidation experiments were repeated on a carboxylic-acid-terminated monolayer on silicon (derived from the hydrolysis of a NHS-UA monolayer, as confirmed by XPS (*vide infra*, Figure 9c) and a water contact angle of ∼39° (in contrast to a contact angle ∼65° for NHS-UA monolayer). This carboxylic-acid-terminated surface displays smaller interaction forces between the surface and the AFM tip

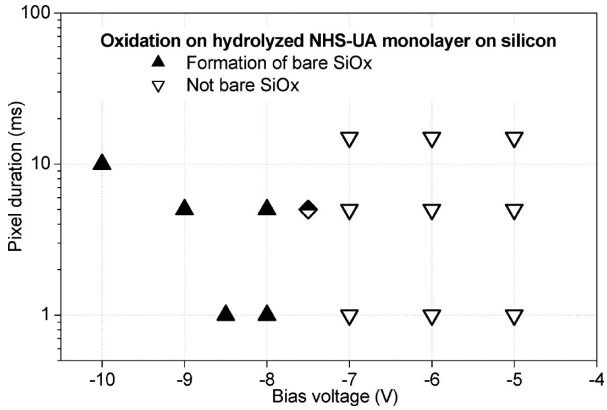

Figure 7. Local probe oxidation results for a hydrolyzed NHS-UA monolayer on silicon. Probe oxidation was carried out at a pixel resolution of 171 pixel/μm). See text for details.

and thus allows straightforward monitoring of the effects of local probe oxidation.

Both the height and friction images of the oxidation patterns on this COOH-terminated monolayer were obtained by contact-mode AFM in both the trace and re-trace scan directions (Figure 7). Biases higher (*i.e.*, more negative) than −7.5 V resulted in the formation of a steady height increase detected by contact-mode AFM. Furthermore, the difference between the apparent heights observed by AFM respectively in trace and re-trace scan directions was very small (typically <0.1 nm), showing the formation of a bare SiO_x protrusion without soft organic coating layer. In contrast, biases smaller (*i.e.*, less negative) than −7.5 V cannot produce steady height changes in contact-mode AFM, implying the presence of a (partially degraded) organic layer.

A bias threshold of −7.5 V cannot reliably produce bare SiO_x protrusions from the hydrolyzed NHS-UA monolayer on silicon. By comparing Figure 7 with Figure 6, these results rule out the possibility of the formation of bare SiO_x protrusions from the NHS-UA monolayer on silicon by biases smaller than −7 V, in line with the conclusion drawn from the oxidation results in Figure 6 that small biases from −3 to −6 V on a NHS-UA monolayer can realize the chemical conversion of the NHS-ester-terminated surface to the carboxyl-terminated surface on the oxidized monolayer.

As schematically illustrated in Figure 5, the significantly higher reactivity of the NHS ester moieties toward amines, compared to that of the carboxylic acid moieties obtained after oxidation, turns the patterned NHS-UA monolayer into an amine-reactive negative-tone template. After the local probe oxidation (Figure 5a,b), the unreacted NHS-ester-terminated surface was functionalized by the reaction with 11-azido-3,6,9-trioxaundecan-1-amine ($N_3-(EO)_3-NH_2$) (Figure 5b,c). The resulting surface was characterized by tapping-mode AFM (Figure 8) and XPS (Figure 9b).

Figure 8 displays tapping-mode AFM height images of the patterned NHS-ester-terminated surface after the

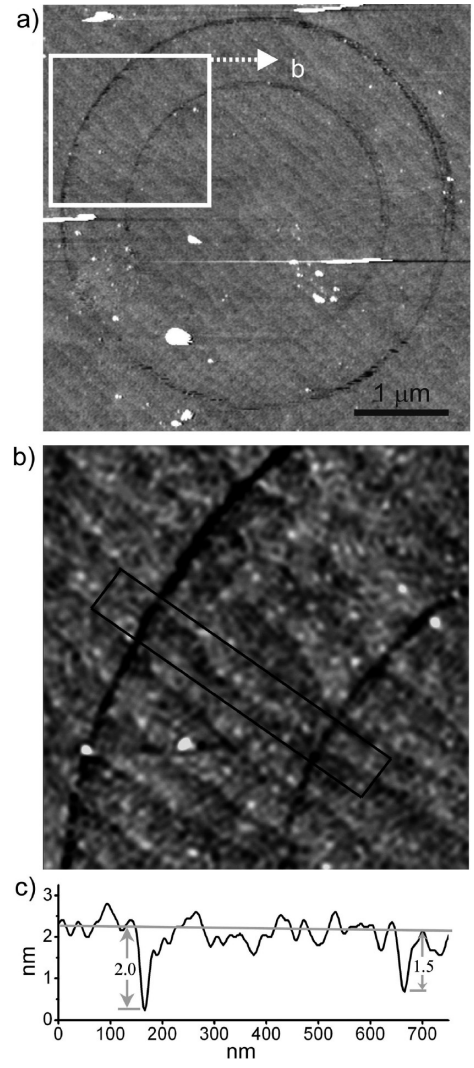

Figure 8. Tapping-mode AFM height images of a locally oxidized NHS-UA monolayer after modification with $H_2N-EO_3-N_3$.

modification with $N_3-(EO)_3-NH_2$ (schematically illustrated as Figure 5c). To minimize any monolayer degradation and SiO_2 formation, such patterned templates with concentric circles were obtained by a −3 V bias. Figure 8 clearly displays most of the inscribed concentric circles with negative heights after the modification with $N_3-(EO)_3-NH_2$ on the surrounding surface (that actually still displays the characteristic atomic terraces of the underlying Si(111) substrate). The observed negative height contrast agrees well with the proposed reaction scheme (Figure 5) in which the oxidized patterns were used as a negative-tone template with diminished chemical reactivity.

The calculated length of the $N_3-(EO)_3-NH-$ moiety is about 1.6 nm (by Chem3D), and thus, taking the previous pattern heights into account, the average depth of the resulting groove-like circles could range from 1.3 to 1.6 nm. However, the apparent depth varies significantly along the inscribed circles: Some parts show an average depth of ~1.5 nm (*e.g.*, the right

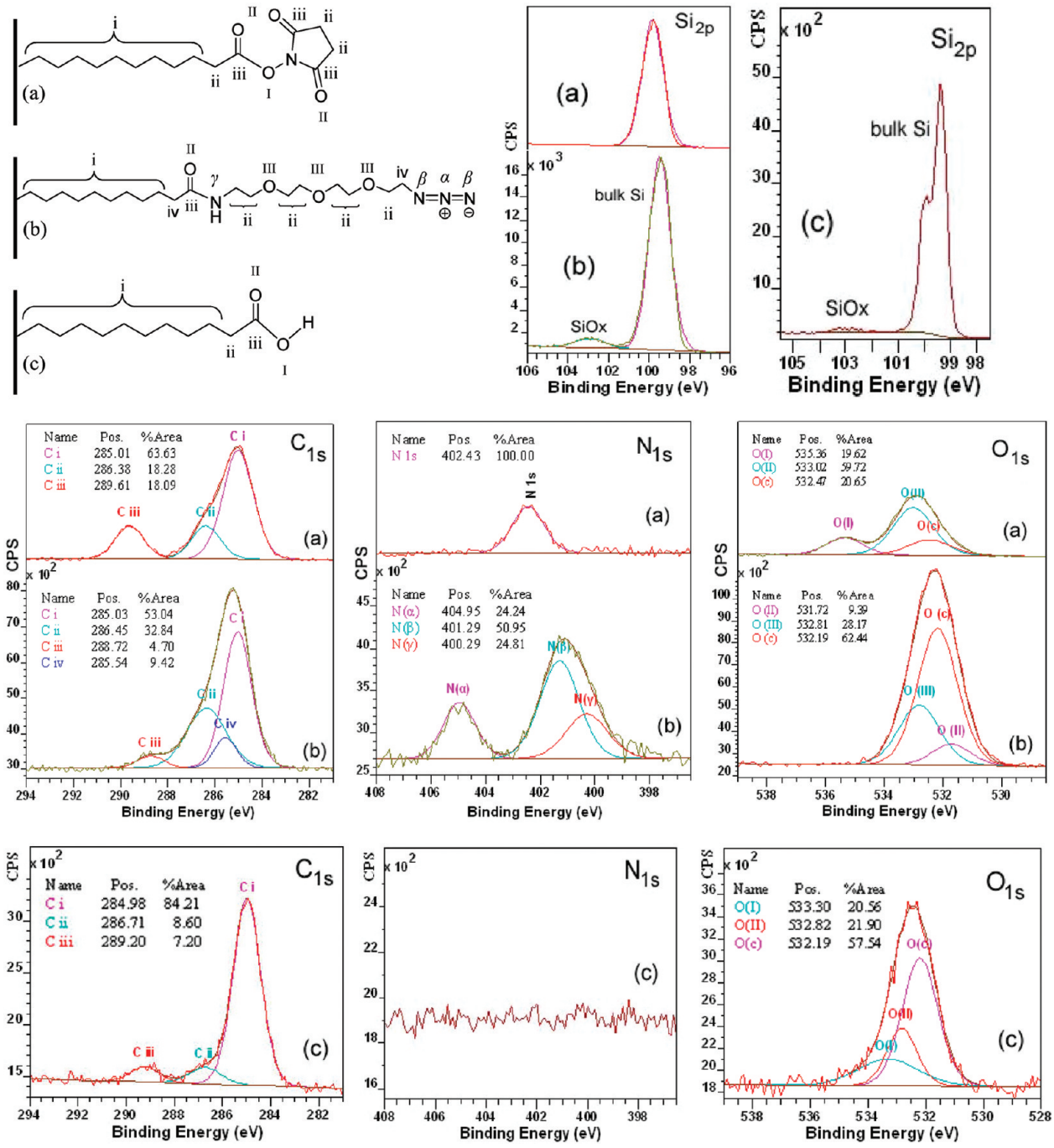

Figure 9. XPS narrow-scan Si_{2p}, C_{1s}, N_{1s}, and O_{1s} spectra and a schematic assignment of a NHS-UA monolayer before (a) and after (b) oxidative lithography and modification with $N_3-(EO)_3-NH_2$, and a hydrolyzed NHS-UA monolayer (c) on silicon. Note: Analyzer pass energy was 16, 20, and 10 eV in spectra (a), (b), and (c), respectively.

groove in Figure 8c), agreeing well with the expected values, while some other parts show a average depth of ~2.0 nm (*e.g.*, the left groove in Figure 8c), a bit larger than the length of $N_3-(EO)_3-NH-$ moiety. One possible explanation for these larger values is that remaining organic layers and/or previously deposited contaminants on the oxidized surface in these parts were (in part) removed by the alkaline solution of $N_3-(EO)_3-NH_2$, leading to an extra increase in the observed depth. Figure 8a also displays some parts of the inscribed circles without a noticeable change in height. This is attributed to the random failure in the preceding probe oxidization on the NHS-ester-terminated surface by the −3 V bias since it is as low as the threshold bias. These inscribed circles have a width of 50−80 nm, in line with the tip radius of ~25 nm.

Finally, the successful attachment of $N_3-(EO)_3-NH_2$ molecules onto the surrounding NHS-ester-terminated surface was also confirmed by XPS spectra. The XPS spectrum of an NHS-UA monolayer on silicon displays several features (Figure 9a):[51] (1) N_{1s} spectrum (a) shows one N_{1s} peak at a binding energy (BE) of 402.4 eV for

the N atom in the cyclic imide of NHS moiety; (2) C_{1s} spectrum (a) shows a peak for three carbonylic carbons (C_{iii}) at a higher BE of 289.6 eV, a peak at 286.4 eV for the α-carbons (C_{ii}) adjacent to the carbonylic carbons, and a peak at 285.0 eV for other carbons (C_i) in the aliphatic hydrocarbon chain. The atomic ratio between the different carbons is $C_i/C_{ii}/C_{iii}$ = 10.6:3:3, agreeing well with the theoretical ratio of 9:3:3 within the experimental error; (3) O_{1s} spectrum (a) shows a small peak at 535.4 eV from the characteristic oxygen atom O_I in the C−O−N bond of the NHS ester moiety and a bigger peak with two components: one at 533.0 eV for the carbonylic oxygen (O_{II}) in the NHS ester moiety (with an atomic ratio of O_I/O_{II} = 1:3) and another one at 532.5 eV for the any unassigned oxygen content (O_c). Furthermore, from these spectra, the atomic ratio of C/N/O_{I+II}(/O) was calculated as 17.2:1:3.9(:4.7) (Table S1a in the Supporting Information), in line with the theoretical ratio of 15:1:4. Since no SiO_x is observed at ~103 eV in Si_{2p} spectrum (a), the excess oxygen as well as carbon likely results from some airborne contaminations absorbed onto the NHS-UA monolayer.

After the oxidative lithography (just in nano/submicrometer size) and the subsequent modification with $N_3-(EO)_3-NH_2$, the modified NHS-UA monolayer displays significant changes in all N_{1s}, C_{1s}, and O_{1s} narrow-scan spectra (b) in Figure 9, which confirmed the cleavage of the NHS ester bonds (to release the NHS moieties) and the consequent formation of amide bonds and attachment of azide groups (Figure 5c). First, in N_{1s} spectrum (b) in Figure 9, the previously present single N_{1s} peak at 402.4 eV for the NHS nitrogen atom in spectrum N_{1s}(a) was replaced with two distinct N_{1s} peaks: the smaller peak for N_α at 405.0 eV from the central, electron-deficient nitrogen in the azide group, while the bigger one at ~401 eV is due to the other two nitrogen atoms in the azide moiety (N_β at 401.3 eV) and the nitrogen in the newly formed amide bond (N_γ at 400.3 eV).[64,65] The integrated atomic ratio of these nitrogen atoms is $N_\alpha/N_\beta/N_\gamma$ = 1:2:1. Furthermore, both C_{1s} and O_{1s} narrow spectra changed in line with the replacement of NHS moieties by target molecules in the monolayer. In comparison with the NHS-UA monolayer, C_{1s} spectrum (b) shows that the carbonylic carbon (C_{iii}) peak shifts to 288.7 eV, while the other three component peaks for the remaining noncarbonylic carbons can be assigned to C_i in the aliphatic hydrocarbon chain at 285.0 eV, C_{ii} bonding to the ether oxygen atom or the amide nitrogen atom at 286.5 eV (these two kinds of carbons are widely reported with chemical shifts of *ca.* 1.3−1.5 eV with respect to the aliphatic carbons C_i[66−68]), and C_{iv} adjacent to the amide carbonyl group or the azide group at 285.5 eV. Among the C_{iv} atoms, the α-carbon adjacent to the carbonylic carbon in a normal amide group was already reported with a chemical shift of ~0.5 eV (quite smaller than that of α-carbons C_{ii} in the NHS-UA monolayer) relative to the aliphatic carbons C_i in organic monolayers.[51,68] As for the carbon atom adjacent to the N_β atom in an azide group,[68] we may assume its BE could be significantly lower than the carbon adjacent to the N_γ atom in an amide group due to the fact that N_β atom presents a higher BE than N_γ, possibly a result of less electron charge withdrawn from the bonded carbon to N_β. The atomic ratio between these carbon atoms is $C_i/C_{ii}/C_{iii}/C_{iv}$ = 11.3:7.0:1:2.0, that is, close to the theoretical ratio of 9:7:1:2. In addition, O_{1s} spectrum (b) displays no peak at ~535 eV, while two component peaks of O_{II} at 531.7 eV and O_{III} at 532.8 eV (with an atomic ratio of O_{II}/O_{III} = 1:3) can be assigned to the carbonylic oxygen in the formed amide bonds and the ether oxygens in the $-(EO)_3-$ moiety, respectively. The atomic ratio of C/N/O_{II+III} is 19.2:4:4 (Table S1b in the Supporting Information), very close to the theoretical ratio of 19:4:4. However, there remains an unassigned component peak of O_c at 532.2 eV due to a large amount of oxygen content from contaminants and the oxidized silicon which was observed at 103 eV in Si_{2p} spectrum (b). The silicon substrate could be oxidized during the oxidative lithography and the subsequent incubation in the basic $N_3-(EO)_3-NH_2$ solution. All these XPS results thus confirm the removal of NHS ester moieties and the attachment of $N_3-(EO)_3-NH_2$ onto the remaining NHS-ester-terminated surface through a newly formed amide bond.

A hydrolyzed NHS-UA monolayer—prepared for the oxidation experiments in Figure 7—was expected to form a largely carboxylic-acid-terminated surface. After a long-term exposure to moist atmosphere, this sample displayed complete loss of the N_{1s} signal (N_{1s} spectrum c), indicating the removal of NHS moieties. Agreeing well with this change, carbon C_{1s} spectrum (c) shows three peaks at 285.0, 286.7, and 289.2 eV, respectively.[69] The atomic ratio between these carbons is $C_i/C_{ii}/C_{iii}$ = 11.7:1.2:1, agreeing well with the theoretical ratio of 9:1:1 for a acid-terminated undecyl monolayer, considering airborne contaminations that can be easily absorbed on this acid-terminated surface. Furthermore, O_{1s} spectrum (c) shows a broad peak at ~532.3 eV, which can be deconvoluted into three components: one at 533.3 eV for the noncarbonylic oxygen (O_I), one at 532.8 eV for the carbonylic oxygen (O_{II}) in the carboxyl group (with a 1:1 ratio for O_I/O_{II}), and a rest peak for other unassigned oxygen components (O_c) (centered at 532.2 eV). The BE of this O_I peak is remarkably lower than that for NHS-UA monolayer (at 535.4 eV). The atomic ratio of C/O_{I+II} is 12.9:2 (Table S1c in the Supporting Information), in good agreement with the theoretical ratio of 11:2. The excess oxygen content (O_c) (with a ratio of 2.7:2 for O_c/O_{I+II}) likely results from some oxygen-rich contaminations absorbed on the monolayer surface, rather than from the small amounts of SiO_x formed during the hydrolysis of the NHS-UA monolayer in moist atmosphere, as only small amounts of

SiO_x were observed at 103 eV in Si_{2p} spectrum (c) in Figure 9. The atomic ratio of C/Si_{ox} (*i.e.*, silicon atoms in the formed SiO_x) is 21.6:1 (Table S1c in the Supporting Information), much greater than a theoretical ratio of C/Si_{top} (*i.e.*, silicon atoms in the top atomic layer on Si(111) substrate) as 11:2 for an undecyl (C_{11}) monolayer on Si(111) upon a substitution percentage of ~50% for the H−Si moieties by C_{11}−Si moieties.[70−72] Therefore, only a small fraction of the unsubstituted H−Si moieties were oxidized into SiO_x beneath the hydrolyzed NHS-UA monolayer. Since this yields only a small disturbance of the Si monolayer interface, it will likely not significantly affect the results of the probe oxidation experiments in Figure 7.

CONCLUSIONS

Local probe oxidation *via* electrically biased AFM tips was successfully applied on covalently Si−C linked hexadecyl and *N*-hydroxysuccinimide (NHS)-ester-terminated undecyl monolayers on unoxidized silicon. The oxidation results—oxidation of the terminal groups of the monolayer and/or formation of silicon oxide—depend on the applied bias voltage and oxidation duration. Like for the local probe oxidation of octadecyl trichlorosilane (OTS) on oxidized silicon (SiO_2/Si), an operational window (typically −4.5 ~ −7 V at 5 ms pixel duration for a hexadecyl monolayer and −3 V at 10 ms pixel duration for a NHS-UA monolayer) exists in which only the monolayer is oxidized. In comparison to the oxidation of OTS monolayer on oxidized silicon, the bias voltage thresholds for the monolayer oxidation are reduced by *ca.* 2 V for a methyl-terminated hexadecyl monolayer and by *ca.* 3.5 V for a NHS-ester-terminated undecyl monolayer on unoxidized silicon.

The mild attachment of highly stable Si−C linked monolayers on H-terminated silicon allows the incorporation of a wide variety of functional groups in the monolayer. This opens up the possibility of even milder local probe oxidations using labile functional groups that can be oxidized at very low bias voltages. It was demonstrated for an NHS-ester-terminated monolayer that application of a bias voltage as low as −3 V yields selective conversion of the terminal groups of the monolayer. Only at significantly larger biases (*e.g.*, −7 V) serious degradation of the monolayer occurs with a concomitant formation of silicon dioxide. By moving an electrically biased tip over an NHS-ester-terminated monolayer, nanopatterns can be inscribed to form negative-tone templates for the subsequent surface modification reaction with amines. This process has been demonstrated by the site-specific coupling of an amine that reacts specifically with the unpatterned background surface, leaving the carbonyl-terminated patterns free for additional reaction steps.

EXPERIMENTAL SECTION

Materials. Single-polished Si(111) (n-type, 500−550 μm thick, resistivity 1−5 Ωcm, miscut angle <0.5°) was purchased from Siltronix Company (France). 1-Hexadecene, 10-undecenoic acid (UA), *N*-hydroxysuccinimide (NHS), dicyclohexyl carbodiimide (DCC), and 11-azido-3,6,9-trioxaundecan-1-amine ($N_3-(CH_2CH_2O)_3CH_2CH_2-NH_2$, abbreviated as $N_3-(EO)_3-NH_2$) were obtained from Aldrich and were used as received. Solvents such as acetone, dichloromethane, chloroform, and 1,2,4-trichlorobenzene were obtained from Aldrich and distilled before use.

Synthesis of *N*-Succinimidyl Undecyl-1-enate (NHS-UA). NHS-UA was synthesized *via* a slight modification of literature procedures.[51,52] In brief, 1-undecylenic acid (UA) (3.68 g; 20 mmol) and NHS (2.53 g; 22 mmol) were dissolved in 100 mL of ethyl acetate, and the resulting mixture was cooled on ice. DCC (4.54 g; 22 mmol) was first dissolved in 2 mL of DMSO and then added to the foregoing solution on ice. The reaction mixture was stored at 4 °C overnight and then quickly washed by saturated brine to completely hydrolyze the remaining DCC. After removal of the water, the organic phase was filtered two times to remove depositions and evaporated under low pressure in a rotavapor to remove solvents. The resulting waxy solid was recrystallized three times from hexane and collected by vacuum filtration with a Büchner funnel. After drying in vacuum overnight, NHS-UA was obtained (3.98 g, 14.1 mmol, yield >70%) with purity of >99% (GC): ^{1}H NMR (300 MHz, $CDCl_3$) δ 5.80 (m, 1H), 4.97 (m, 2H), 2.85 (s, 4H), 2.62 (t, 2H), 2.05 (q, 2H), 1.76 (m, 2H), 1.33−1.42 (m, 10H).

Si(111) Etching and Monolayer Preparation. The detailed procedures to prepare NHS-UA and hexadecyl monolayers on silicon were previously described.[26,51] In brief, the oxygen plasma-cleaned chips of Si(111) wafer were etched into a H-terminated surface by immersing in an argon-saturated 40% aqueous NH_4F solution for 15 min under an argon atmosphere. Both hexadecyl and NHS-UA monolayers were, respectively, prepared by immersing the freshly prepared H-terminated Si(111) chips into a deoxygenated 0.4 M solution of hexadecene or NHS-UA in 1,2,4-trichlorobenzene, followed by irradiation with 447 nm light for 20 h. After cleaning by extensive sonication in dichloromethane, samples were dried in a stream of nitrogen. A hydrolyzed NHS-UA monolayer on silicon was obtained by storing a NHS-UA monolayer in a sealed air atmosphere over water for 6 months (shorter times may also be sufficient, but this has not been tested). It was cleaned by sonication in dichloromethane, acetone, ethanol, and water and dried in a stream of nitrogen.

Equipment. AFM imaging and local probe oxidation experiments were performed on a NTEGRA SPM (NT-MDT, Moscow, Russia). AFM images were recorded in 512 × 512 pixel resolution. Contact angle measurements were carried out on a DSA 100 (KRÜSS, Germany). The XPS analysis was performed with a JPS-9200 photoelectron spectrometer (JEOL, Japan) under UHV conditions (~5 × 10^{-7} Pa) using a monochromatic Al Kα X-ray radiation source at 12 kV and 25 mA at a takeoff angle of 80°. The high-resolution spectra were obtained at pass energies of 10−20 eV as mentioned in text, while for wide-scan spectra, a pass energy of 50 eV was used. The measuring spots are 3 mm in diameter. The obtained XPS data were processed using CasaXPS.

Local Probe Oxidation. Oxidation experiments were performed in contact mode in ambient conditions at 30−40% relative humidity. The silicon substrate of samples was solidly grounded. A conductive AFM tip was controlled by a vector scan program (new version for Windows compared to pixel-based DOS software used in ref 12) to continuously move along the preprogrammed routes and be biased to realize the oxidation lithography in one sweep. The tip moving speed (*S*, μm/s) in our vector scan program was set in a combinational manner of pixel resolution (*R*, pixel/μm) with pixel duration (*t*, ms/pixel), that is, $S = 1000/(R \times t)$. We did the oxidation with varying pixel duration (0.1−10 ms/pixel) at pixel resolution of 512 pixels over 2500 nm length (~205 pixels/μm) on hexadecyl monolayers and 512 pixels over

3000 nm length (~171 pixel/μm) on NHS-UA and its hydrolyzed monolayers.

Since oxidation results, for example, the exact oxidation threshold, are known to depend on the tip quality and tip material, all oxidation experiments were performed without prescanning of the target area to reduce tip-wear influences. Conductive AFM probes were all coated by a Pt layer. In detail, for oxidation and imaging on hexadecyl and hydrolyzed NHS-UA monolayers, Pt-coated CSG01 type probes (from NT-MDT, tip radius ~35 nm, force constant $k \sim 0.03$ N/m, $f \sim 9.8$ kHz, $L \sim 350$ μm) were used in contact mode. Height and friction images were recorded in both the trace and re-trace scan directions just after oxidation lithography. On NHS-UA monolayers, Pt-coated NSC36(-A) type probes (from Mikromasch; tip radius ~25 nm, $k \sim 0.95$ N/m, $f \sim 105$ kHz, $L \sim 110$ μm) were used in contact mode for oxidation lithography and in tapping mode for imaging just after oxidation lithography.

Coupling of 11-azido-3,6,9-trioxaundecan-1-amine to NHS-ester-terminated monolayers was performed by placing the patterned wafers in a 1 mM CH_2Cl_2 solution overnight followed by thorough rinsing with CH_2Cl_2 and drying in a nitrogen gas stream. The resulting surface was imaged by AFM in tapping mode with an uncoated NSG36-type probe.

Acknowledgment. D.W. and U.S.S. thank the Dutch Polymer Institute (DPI), NWO, and the Fonds der Chemischen Industrie for financial support. M.Y. and H.Z. thank NanoNed, funded by the Dutch Ministry of Economic Affairs (Project WSC.6972), for financial support.

Supporting Information Available: AFM image of the NHS-UA monolayer; XPS spectra and elemental contents of the hexadecyl monolayer, the NHS-UA monolayer, the hydrolyzed NHS-UA monolayer, and the patterned and $N_3-(EO)_3-NH_2$ modified NHS-UA monolayer. HF-etching experiments. This material is available free of charge *via* the Internet at http://pubs.acs.org.

REFERENCES AND NOTES

1. Snow, E. S.; Campbell, P. M. Fabrication of Si Nanostructures with an Atomic Force Microscope. *Appl. Phys. Lett.* **1994**, *64*, 1932–1934.
2. Day, H. C.; Allee, D. R. Selective Area Oxidation of Silicon with a Scanning Force Microscope. *Appl. Phys. Lett.* **1993**, *62*, 2691–2693.
3. Dagata, J. A. Device Fabrication by Scanned Probe Oxidation. *Science* **1995**, *270*, 1625–1626.
4. Wouters, D.; Hoeppener, S.; Schubert, U. S. Local Probe Oxidation of Self-assembled Monolayers: Templates for the Assembly of Functional Nanostructures. *Angew. Chem., Int. Ed.* **2009**, *48*, 1732–1739.
5. Using soft lithography, for example: Onclin, S.; Ravoo, B.-J.; Reinhoudt, D. N. Engineering Silicon Oxide Surfaces Using Self-Assembled Monolayers. *Angew. Chem., Int. Ed.* **2005**, *44*, 6282–6304.
6. Using photochemical patterning, for example: ter Maat, J.; Regeling, R.; Yang, M.; Mullings, M. N.; Bent, S. F.; Zuilhof, H. Photochemical Covalent Attachment of Alkene-Derived Monolayers onto Hydroxyl-Terminated Silica. *Langmuir* **2009**, DOI: 10.1021/la901551t.
7. Kim, B.; Park, H.; Lee, S.-H.; Sigmund, W. M. The Effect of Monolayers' Alkyl Chain Length on Atomic Force Microscopy Anodization Lithography. *Colloids Surf., A* **2005**, *253*, 23–26.
8. Sugimura, H.; Hanji, T.; Hayashi, K.; Takai, O. Surface Potential Nanopatterning Combining Alkyl and Fluoroalkylsilane Self-Assembled Monolayers Fabricated *via* Scanning Probe Lithography. *Adv. Mater.* **2002**, *14*, 524–526.
9. Maoz, R.; Cohen, S. R.; Sagiv, J. Nanoelectrochemical Patterning of Monolayer Surfaces: Toward Spatially Defined Self-Assembly of Nanostructures. *Adv. Mater.* **1999**, *11*, 55–61.
10. Maoz, R.; Frydman, E.; Cohen, S. R.; Sagiv, J. "Constructive Nanolithography": Inert Monolayers as Patternable Templates for *In-Situ* Nanofabrication of Metal-Semiconductor-Organic Surface Structures—A Generic Approach. *Adv. Mater.* **2000**, *12*, 725–731.
11. Wouters, D.; Schubert, U. S. Constructive Nanolithography and Nanochemistry: Local Probe Oxidation and Chemical Modification. *Langmuir* **2003**, *19*, 9033–9038.
12. Wouters, D.; Willems, R.; Hoeppener, S.; Flipse, C. F. J.; Schubert, U. S. Oxidation Conditions for Octadecyl Trichlorosilane Monolayers on Silicon: A Detailed Atomic Force Microscopy Study of the Effects of Pulse Height and Duration on the Oxidation of the Monolayer and the Underlying Si Substrate. *Adv. Funct. Mater.* **2005**, *15*, 938–944.
13. Hoeppener, S.; Maoz, R.; Cohen, S. R.; Chi, L. F.; Fuchs, H.; Sagiv, J. Metal Nanoparticles, Nanowires, and Contact Electrodes Self-Assembled on Patterned Monolayer Templates—A Bottom-Up Chemical Approach. *Adv. Mater.* **2002**, *14*, 1036–1041.
14. Linford, M. R.; Chidsey, C. E. D. Alkyl Monolayers Covalently Bonded to Silicon Surfaces. *J. Am. Chem. Soc.* **1993**, *115*, 12631–12632.
15. Hacker, C. A.; Anderson, K. A.; Richter, L. J.; Richter, C. A. Comparison of Si−O−C Interfacial Bonding of Alcohols and Aldehydes on Si(111) Formed from Dilute Solution with Ultraviolet Irradiation. *Langmuir* **2005**, *21*, 882–889.
16. Gergel-Hackett, N.; Zangmeister, C. D.; Hacker, C. A.; Richter, L. J.; Richter, C. A. Demonstration of Molecular Assembly on Si (100) for CMOS-Compatible Molecule-Based Electronic Devices. *J. Am. Chem. Soc.* **2008**, *130*, 4259–4261.
17. Sieval, A. B.; Linke, R.; Zuilhof, H.; Sudholter, E. J. R. High-Quality Alkyl Monolayers on Silicon Surfaces. *Adv. Mater.* **2000**, *12*, 1457–1460.
18. Buriak, J. M. Organometallic Chemistry on Silicon and Germanium Surfaces. *Chem. Rev.* **2002**, *102*, 1271–1308.
19. Wayner, D. D. M.; Robert, A.; Wolkow, R. A. Organic Modification of Hydrogen Terminated Silicon Surfaces. *J. Chem. Soc., Perkin Trans. 2* **2002**, 23–34.
20. Hamers, R. J. Formation and Characterization of Organic Monolayers on Semiconductor Surfaces. *Annu. Rev. Anal. Chem.* **2008**, *1*, 707–36.
21. Voicu, R.; Boukherroub, R.; Bartzoka, V.; Ward, T.; Wojtyk, J. T. C.; Wayner, D. D. M. Formation, Characterization, and Chemistry of Undecanoic Acid-Terminated Silicon Surfaces: Patterning and Immobilization of DNA. *Langmuir* **2004**, *20*, 11713–11720.
22. Faucheux, A.; Gouget-Laemmel, A. C.; Henry de Villeneuve, C.; Boukherroub, R.; Ozanam, F.; Allongue, P.; Chazalviel, J.-N. Well-Defined Carboxyl-Terminated Alkyl Monolayers Grafted onto H-Si(111): Packing Density from a Combined AFM and Quantitative IR Study. *Langmuir* **2006**, *22*, 153–162.
23. Linford, M. R.; Fenter, P.; Eisenberger, P. M.; Chidsey, C. E. D. Alkyl Monolayers on Silicon Prepared from 1-Alkenes and Hydrogen-Terminated Silicon. *J. Am. Chem. Soc.* **1995**, *117*, 3145–3155.
24. Sieval, A. B.; Demirel, A. L.; Nissink, J. W. M.; Linford, M. R.; Van der Maas, J. H.; De Jeu, W. H.; Zuilhof, H.; Sudhölter, E. J. R. Highly Stable Si−C Linked Functionalized Monolayers on the Silicon (100) Surface. *Langmuir* **1998**, *14*, 1759–1768.
25. Cicero, R. L.; Linford, M. R.; Chidsey, C. E. D. Photoreactivity of Unsaturated Compounds with Hydrogen-Terminated Silicon(111). *Langmuir* **2000**, *16*, 5688–5695.
26. Sun, Q.-Y.; De Smet, L. C. P. M.; Van Lagen, B.; Wright, A.; Zuilhof, H.; Sudhölter, E. J. R. Covalently Attached Monolayers on Hydrogen-Terminated Si(100): Extremely Mild Attachment by Visible Light. *Angew. Chem., Int. Ed.* **2004**, *43*, 1352–1355.
27. Sun, Q.-Y.; De Smet, L. C. P. M.; Van Lagen, B.; Giesbers, M.; Thüne, P. C.; Van Engelenburg, J.; De Wolf, F. A.; Zuilhof, H.; Sudhölter, E. J. R. Covalently Attached Monolayers on Crystalline Hydrogen-Terminated Silicon: Extremely Mild Attachment by Visible Light. *J. Am. Chem. Soc.* **2005**, *127*, 2514–2523.

28. Scheres, L.; Achten, R.; Giesbers, M.; de Smet, L. C. P. M.; Arafat, A.; Sudhölter, E. J. R.; Marcelis, A. T. M.; Zuilhof, H. Covalent Attachment of Bent-Core Mesogens to Silicon Surfaces. *Langmuir* **2009**, *25*, 1529–1533.
29. Scheres, L.; Arafat, A.; Zuilhof, H. Self-Assembly of High-Quality Covalently Bound Organic Monolayers onto Silicon. *Langmuir* **2007**, *23*, 8343–8346.
30. Buriak, J. M.; Stewart, M. P.; Geders, T. W.; Allen, M. J.; Choi, H. C.; Smith, J.; Raftery, D.; Canham, L. T. Lewis Acid Mediated Hydrosilylation on Porous Silicon Surfaces. *J. Am. Chem. Soc.* **1999**, *121*, 11491–11502.
31. Faber, E. J.; Sparreboom, W.; Groeneveld, W.; De Smet, L. C. P. M.; Olthuis, W.; Zuilhof, H.; Sudhölter, E. J. R.; Bergveld, P.; Van der Berg, A. pH Sensitivity of Si-C Linked Organic Monolayers on Crystalline Silicon Surfaces. *ChemPhysChem* **2007**, *8*, 101–112.
32. Faber, E. J.; De Smet, L. C. P. M.; Olthuis, W.; Zuilhof, H.; Sudhölter, E. J. R.; Bergveld, P.; Van der Berg, A. Si−C Linked Organic Monolayers on Crystalline Silicon Surfaces as Alternative Gate Insulators. *ChemPhysChem* **2005**, *6*, 2153–2166.
33. Sieval, A. B.; Huisman, C. L.; Schonecker, A.; Schuurmans, F. M.; van der Heide, A. S. H.; Goossens, A.; Sinke, W. C.; Zuilhof, H.; Sudhölter, E. J. R. Silicon Surface Passivation by Organic Monolayers: Minority Charge Carrier Lifetime Measurements and Kelvin Probe Investigations. *J. Phys. Chem. B* **2003**, *107*, 6846–6852.
34. Liu, Y.-J.; Yu, H.-Z. Molecular Passivation of Mercury-Silicon (p-type) Diode Junctions: Alkylation, Oxidation, and Alkylsilation. *J. Phys. Chem. B* **2003**, *107*, 7803–7811.
35. Bansal, A.; Lewis, N. S. Electrochemical Properties of (111)-Oriented n-Si Surfaces Derivatized with Covalently-Attached Alkyl Chains. *J. Phys. Chem. B* **1998**, *102*, 1067–1070.
36. Royea, W. J.; Juang, A.; Lewis, N. S. Preparation of Air-Stable, Low Recombination Velocity Si(111) Surfaces through Alkyl Termination. *Appl. Phys. Lett.* **2000**, *77*, 1988–1990.
37. Webb, L. J.; Lewis, N. S. Comparison of the Electrical Properties and Chemical Stability of Crystalline Silicon(111) Surfaces Alkylated Using Grignard Reagents or Olefins with Lewis Acid Catalysts. *J. Phys. Chem. B* **2003**, *107*, 5404–5412.
38. Kar, S.; Miramond, C.; Vuillaume, D. Properties of Electronic Traps at Silicon/1-Octadecene Interfaces. *Appl. Phys. Lett.* **2001**, *78*, 1288–1290.
39. Miramond, C.; Vuillaume, D. 1-Octadecene Monolayers on Si(111) Hydrogen-Terminated Surfaces: Effect of Substrate Doping. *J. Appl. Phys.* **2004**, *96*, 1529–1536.
40. Yaffe, O.; Scheres, L.; Puniredd, S. R.; Stein, N.; Biller, A.; Lavan, R. H.; Shpaisman, H.; Zuilhof, H.; Haick, H.; Cahen, D.; Vilan, A. Molecular Electronics at Metal/Semiconductor Junctions. Si Inversion by Sub-Nanometer Molecular Films. *Nano Lett.* **2009**, *9*, 2390–2394.
41. Wang, W.; Scott, A.; Gergel-Hackett, N.; Hacker, C. A.; Janes, D. B.; Richter, C. A. Probing Molecules in Integrated Silicon−Molecule−Metal Junctions by Inelastic Tunneling Spectroscopy. *Nano Lett.* **2008**, *8*, 478–484.
42. Ara, M.; Graaf, H.; Tada, H. Nanopatterning of Alkyl Monolayers Covalently Bound to Si(111) with an Atomic Force Microscope. *Appl. Phys. Lett.* **2002**, *80*, 2565–2567.
43. Ara, M.; Tada, H. Friction Force Microscopy Using Silicon Cantilevers Covered with Organic Monolayers *via* Silicon−Carbon Covalent Bonds. *Appl. Phys. Lett.* **2003**, *83*, 578–580.
44. Okada, R.; Miyadera, T.; Shimada, T.; Koma, A.; Ueno, K.; Saiki, K. Methyl-Terminated Si(111) Surface as the Ultra Thin Protection Layer to Fabricate Position-controlled Alkyl SAMs by Using Atomic Force Microscope Anodic Oxidation. *Surf. Sci.* **2004**, *552*, 46–52.
45. Yang, M.; Zheng, Z.; Liu, Y.; Zhang, B. Kinetics of Atomic Force Microscope-Based Scanned Probe Oxidation on an Octadecylated Silicon (111) Surface. *J. Phys. Chem. B* **2006**, *110*, 10365–10373.
46. Yang, M.; Zheng, Z.; Liu, Y.; Zhang, B. Scanned Probe Oxidation on an Octadecyl-Terminated Silicon(111) Surface with Atomic Force Microscopy: Kinetic Investigations in Line Patterning. *Nanotechnology* **2006**, *17*, 330–337.
47. Pignataro, B.; Licciardello, A.; Cataldo, S.; Marletta, G. SPM and TOF-SIMS Investigation of the Physical and Chemical Modification Induced by Tip Writing of Self-Assembled Monolayers. *Mater. Sci. Eng., C* **2003**, *23*, 7–12.
48. Gu, J.; Yam, C. M.; Li, S.; Cai, C. Nanometric Protein Arrays on Protein-Resistant Monolayers on Silicon Surfaces. *J. Am. Chem. Soc.* **2004**, *126*, 8098–8099.
49. Fresco, Z. M.; Suez, I.; Backer, S. A.; Fréchet, J. M. J. AFM-Induced Amine Deprotection: Triggering Localized Bond Cleavage by Application of Tip/Substrate Voltage Bias for the Surface Self-Assembly of Nanosized Dendritic Objects. *J. Am. Chem. Soc.* **2004**, *126*, 8374–8375.
50. Fresco, Z. M.; Fréchet, J. M. J. Selective Surface Activation of a Functional Monolayer for the Fabrication of Nanometer Scale Thiol Patterns and Directed Self-Assembly of Gold Nanoparticles. *J. Am. Chem. Soc.* **2005**, *127*, 8302–8303.
51. Yang, M.; Teeuwen, R. L. M.; Giesbers, M.; Baggerman, J.; Arafat, A.; De Wolf, F. A.; Van Hest, J. C. M.; Zuilhof, H. One-Step Photochemical Attachment of NHS-Terminated Monolayers onto Silicon Surfaces and Subsequent Functionalization. *Langmuir* **2008**, *24*, 7931–7938.
52. Böcking, T.; James, M.; Coster, H. G. L.; Barrow, K. D. Structural Characterization of Organic Multilayers on Silicon(111) Formed by Immobilization of Molecular Films on Functionalized Si−C Linked Monolayers. *Langmuir* **2004**, *20*, 9227–9235.
53. Ishizaki, T.; Saito, N.; SunHyung, L.; Ishida, K.; Takai, O. Study of Alkyl Organic Monolayers with Different Molecular Chain Lengths Directly Attached to Silicon. *Langmuir* **2006**, *22*, 9962–9966.
54. Kopycinska-Müller, M.; Geiss, R. H.; Hurley, D. C. Contact Mechanics and Tip Shape in AFM-Based Nanomechanical Measurements. *Ultramicroscopy* **2006**, *106*, 466–474.
55. Fontaine, P. A.; Dubois, E.; Stiévenard, D. Characterization of Scanning Tunneling Microscopy and Atomic Force Microscopy-Based Techniques for Nanolithography on Hydrogen-Passivated Silicon. *J. Appl. Phys.* **1998**, *84*, 1776–1781.
56. Teuschler, T.; Mahr, K.; Miyazaki, S.; Hundhausen, M.; Ley, L. Nanometer-Scale Field Induced Oxidation of Si(111)-H by a Conducting-Probe Scanning Force Microscope: Doping Dependence and Kinetics. *Appl. Phys. Lett.* **1995**, *67*, 3144–3146.
57. Ley, L.; Teuscler, T.; Mahr, K.; Miyazaki, S.; Hundhausen, M. Kinetics of Field-Induced Oxidation of Hydrogen-Terminated Si(111) by Means of a Scanning Force Microscope. *J. Vac. Sci. Technol., B* **1996**, *14*, 2845–2849.
58. Morimoto, K.; Pérez-Murano, F.; Dagata, J. A. Density Variations in Scanned Probe Oxidation. *Appl. Surf. Sci.* **2000**, *158*, 205–216.
59. Dagata, J. A.; Inoue, T.; Itoh, J.; Matsumoto, K.; Yokoyama, H. Role of Space Charge in Scanned Probe Oxidation. *J. Appl. Phys.* **1998**, *84*, 6891–6900.
60. Dagata, J. A.; Perez-Murano, F.; Martin, C.; Kuramochi, H.; Yokoyama, H. Current, Charge, and Capacitance during Scanning Probe Oxidation of Silicon. I. Maximum Charge Density and Lateral Diffusion. *J. Appl. Phys.* **2004**, *96*, 2386–2392.
61. Sugimura, H.; Hanji, T.; Hayashi, K.; Takai, O. Surface Modification of an Organosilane Self-Assembled Monolayer on Silicon Substrates Using Atomic Force Microscopy: Scanning Probe Electrochemistry toward Nanolithography. *Ultramicroscopy* **2002**, *91*, 221–226.
62. Ahn, S.-J.; Jang, Y.-K.; Lee, H.; Lee, H. Mechanism of Atomic Force Microscopy Anodization Lithography on a Mixed Langmuir−Blodgette Resist of Palmitic Acid And Hexadecylamine on Silicon. *Appl. Phys. Lett.* **2002**, *80*, 2592–2594.

63. Lee, H.; Kim, S.-A.; Ahn, S.-J.; Lee, H. Positive and Negative Patterning on a Palmitic Acid Langmuir−Blodgett Monolayer on Si Surface Using Bias-Dependent Atomic Force Microscopy Lithography. *Appl. Phys. Lett.* **2002**, *81*, 138–140.
64. Collman, J. P.; Devaraj, N. K.; Eberspacher, T. P. A.; Chidsey, C. E. D. Mixed Azide-Terminated Monolayers: A Platform for Modifying Electrode Surfaces. *Langmuir* **2006**, *22*, 2457–2464.
65. Haensch, C.; Hoeppener, S.; Schubert, U. S. Chemical Surface Reactions by Click Chemistry: Coumarin Dye Modification of 11-Bromoundecyltrichlorosilane Monolayers. *Nanotechnology* **2008**, *19*, 035703.
66. Sharma, S.; Johnson, R. W.; Desai, T. A. XPS and AFM Analysis of Antifouling PEG Interfaces for Microfabricated Silicon Biosensors. *Biosens. Bioelectron.* **2004**, *20*, 227–239.
67. Cecchet, F.; De Meersman, B.; Demoustier-Champagne, S.; Nysten, B.; Jonas, A. M. One Step Growth of Protein Antifouling Surfaces: Monolayers of Poly(ethylene oxide) (PEO) Derivatives on Oxidized and Hydrogen-Passivated Silicon Surfaces. *Langmuir* **2006**, *22*, 1173–1181.
68. Brigss, D., Grant, J. T., Eds. *Surface Analysis by Auger and X-ray Photoelectron Spectroscopy*; IM Publications: Chichester, U.K., 2003.
69. Strother, T.; Cai, W.; Zhao, X.; Hamers, R. J.; Smith, L. M. Synthesis and Characterization of DNA-Modified Silicon (111) Surfaces. *J. Am. Chem. Soc.* **2000**, *122*, 1205–1209.
70. Sieval, A. B.; van den Hout, B.; Zuilhof, H.; Sudhölter, E. J. R. Molecular Modeling of Covalently Attached Alkyl Monolayers on the Hydrogen-Terminated Si(111) Surface. *Langmuir* **2001**, *17*, 2172–2181.
71. Zhang, L.; Wesley, K.; Jiang, S. Molecular Simulation Study of Alkyl Monolayers on Si(111). *Langmuir* **2001**, *17*, 6275–6281.
72. Pei, Y.; Ma, J.; Jiang, Y. Formation Mechanisms and Packing Structures of Alkoxyl and Alkyl Monolayers on Si(111): Theoretical Studies with Quantum Chemistry and Molecular Simulation Models. *Langmuir* **2003**, *19*, 7652–7661.